Chapter 6
Vision-Based Line Tracking Control and Stability Analysis of Unicycle Mobile Robots

Plamen Petrov and Veska Georgieva

Abstract This paper addresses the problem of vision-based line tracking control of unicycle mobile robots. First, a robot-camera model suitable for path following applications is derived. Using a look-ahead approach, a feedback controller is proposed for tracking curved paths on the ground using information from an onboard down-looking camera using distance-only measurements. Stability properties of the closed-loop system are analyzed, and asymptotic stability of the resulting closed-loop control system is proved using Lyapunov stability theory. Simulation and experimental results are presented to illustrate the effectiveness of the proposed control scheme.

6.1 Introduction

In the last decades, the wheeled mobile robots (WMRs) have been increasingly used in wide range of applications, such as in factories [1], as service robots [2], autonomous vehicles [3], exploration robots [4], for military operations [5], and research [6]. At control level, important results have been established concerning three fundamental motion control tasks, namely point stabilization (the parking problem), trajectory tracking, and path following [7]. In what concerns the path following problem, in contrast of trajectory tracking, the mobile robot has to follow and to converge to a reference path, which is given without temporal specification. The path following control of mobile robot has been intensively studied during the years, and different solutions have been proposed in the literature, such as nonlinear [8] and linear controllers [9]. When designing controllers for path tracking applications, often the curvature of the reference path is considered a priori known, which

P. Petrov (✉) · V. Georgieva
Technical University of Sofia, Sofia 1000, Bulgaria
e-mail: ppetrov@tu-sofia.bg

V. Georgieva
e-mail: vesg@tu-sofia.bg

R. Kountchev et al. (eds.), *New Approaches for Multidimensional Signal Processing*,
Smart Innovation, Systems and Technologies 216,
https://doi.org/10.1007/978-981-33-4676-5_6

permits to introduce it directly in the control law, simplifying the design of the controller [10]. In this case, it is also considered that both measurements for the lateral and orientation errors are available for feedback control design [11]. However, depending of the assigned mobile robot guiding point, using look-ahead approach [12], it is possible to use only distance measurements for the lateral offset from the reference line without using data for the orientation error, which considerably simplify the controller design. The advantage of using such approach is considerable in the case, when the mobile robot has to follow a path with unknown curvature and avoids its direct calculation, which involves higher-order derivative computation. In addition, calculation of the orientation error between the mobile robot and the reference path avoided, which considerably simplifies the structure of the controller.

The use of visual information in the feedback loop has been an attractive solution for the motion control of mobile robots and different visual servo algorithms have been developed over the last decades. The control based of visual measurements is termed visual servoing or vision-based control and two main approaches are distinguished, namely position-based visual servoing (PBVS) and image-based visual servoing (IBVS) [13]. In the PBVS approach, three-dimensional scene information is used and the feedback is based on the pose estimation of the observed object with respect to the camera in order to regulate the motion of the onboard camera to a desired pose [14–16]. For path following applications, a specific feature is that the error coordinates with respect to the desired path to follow are computed in the task space. In the IBVS approach, the pose estimation is omitted, image features are used as the state in the control, such that the error coordinates are measured in the image, and the control law is directly expressed in the image plane and mapped to actuator commands [17–19].

In this paper, we deal with the problem of path tracking control for nonholonomic unicycle WMRs, which use monocular vision guided system for line tracking. The reference path is assumed to be a sequence of circular and/or straight-line segments, where the curvatures of the circular segments are not known. The look-ahead approach [12, 15] used in this paper consists of tracking a reference path with a guiding reference point in front of robot at a given distance ahead from the wheel axle. For this end, first, a robot-camera model of the robot using the look-ahead reference point is derived. A linear controller is designed using lateral error-only measurements without involving values of the path curvature (which is unknown) or the orientation error with respect to the reference path. Based on Lyapunov stability theory, the stability property of the synthesized system is analyzed. Some simulation and experimental results are given, in order to demonstrate the validity of the designed controller.

6.2 Model Development

6.2.1 Robot Kinematic Model

A plane view of a unicycle mobile robot, considered in this paper, which is moving on a horizontal plane, is shown in Fig. 6.1. A monocular camera is placed on the robot pointing downward perpendicular to the ground. For simplicity of exposition, for path following applications, we will use two-dimensional (2D) Cartesian coordinate systems instead 3D systems, where it is possible. With reference to Fig. 6.1, in order to describe the path tracking kinematics, the following coordinate systems are defined: an inertial coordinate system Fxy; a robot coordinate system Px_Py_P located at the mid-point of the wheel axle with x_P axis directed along the longitudinal base of the robot; a robot coordinate system Rx_Ry_R attached firmly to the robot at a distance h from the ground and at a distance d ahead from point P, in such way that the x_R-axis is aligned with x_P-axis of Px_Py_P; a camera frame Cx_Cy_C which center is placed in the optical center of the camera and coincides with the center of the robot frame Rx_Ry_R; and a moving virtual reference frame Lx_Ly_L associated with the reference line to follow, with a center L assigned in the intersection between the y_R-axis of Rx_Ry_R and the reference path, such that the x_L-axis is tangent to the path and oriented in the direction of motion. The look-ahead point R is defined as a robot guided (reference) point for the line tracking scenario.

Let us denote the coordinates of point P in the fixed frame Fxy as

$$^F p_P = \begin{bmatrix} x_P & y_P \end{bmatrix}^T \tag{6.1}$$

where $^F p_P \in R^2$, and the orientation of the robot in Fxy as $\psi \in S^1$. The kinematic equations of motion of the unicycle mobile robot under the nonholonomic constraints

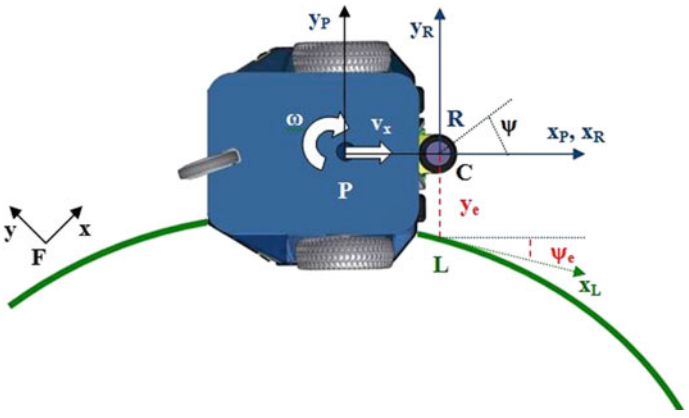

Fig. 6.1 Geometry of the line tracking scenario

of pure rolling and nonslipping can be written as follows [12]

$$\dot{\widehat{p}}_P = B_P \eta, \tag{6.2}$$

where $\dot{\widehat{p}}_P$ represents the time derivative of $\widehat{p}_P \in R^2 \times S^1$, defined as

$$\widehat{p}_P = \begin{bmatrix} x_P & y_P & \psi \end{bmatrix}^T, \tag{6.3}$$

which is a vector of the posture coordinates of the robot using the reference point P, the transformation matrix $B_P \in R^{3\times 2}$ is given by

$$B_P = \begin{bmatrix} \cos\psi & 0 \\ \sin\psi & 0 \\ 0 & 1 \end{bmatrix},$$

and the vector $\eta \in \Re^2$

$$\eta = \begin{bmatrix} v_{Px} & \omega \end{bmatrix}^T \tag{6.4}$$

is composed of the robot linear and angular velocities denoted by $v_{Px} \in \Re$ and $\omega \in \Re$, respectively.

Denoting with ${}^F p_R \in \Re^2$ a vector representing the coordinates of point R with respect to Fxy

$${}^F p_R = \begin{bmatrix} x_R & y_R \end{bmatrix}^T, \tag{6.5}$$

and with ${}^P d = \begin{bmatrix} {}^P d_x & 0 \end{bmatrix}^T \in \Re^2$ a vector from point P to point R expressed in the coordinate frame Px_Py_P, using (6.1) the coordinates of points R and P are related by

$${}^F p_R = {}^F p_P + R(\psi)\,{}^P d, \tag{6.6}$$

where $R(\psi) \in SO(2)$ is an orthogonal rotation matrix of angle ψ, (ψ is the orientation angle of the robot with respect to fixed frame Fxy), given by

$$R(\psi) = \begin{bmatrix} \cos\psi & -\sin\psi \\ \sin\psi & \cos\psi \end{bmatrix}.$$

Differentiating (6.6) with respect to time, one obtains

$$
\begin{aligned}
{}^{F}\dot{p}_R &= R(\psi)\left({}^{P}\dot{p}_P + \omega S(\pi/2)\,{}^{P}d\right) \\
&= G\eta,
\end{aligned} \tag{6.7}
$$

where $G = R(\psi)D \in \Re^{2\times 2}$ with $D \in \Re^{2\times 2}$ given by

$$
D = \begin{bmatrix} 1 & 0 \\ 0 & {}^{P}d_x \end{bmatrix},
$$

$S(\pi/2) \in SS(2)$ is a skew symmetric matrix and ${}^{P}\dot{p}_P = \left[v_{Px}, v_{Py}\right]^T \in R^2$ is a vector of the projections of the velocity of point P relative to the fixed coordinate system Fxy on the axes of the moving robot coordinate system Px_Py_P.

In order to express the robot kinematic model using the coordinates (6.5) of point R in an inertial frame Fxy, we define a vector of the posture coordinates ${}^{F}\widehat{p}_R \in R^2 \times S^1$, as follows

$$
{}^{F}\widehat{p}_R = \left[x_R \;\; y_R \;\; \psi\right]^T. \tag{6.8}
$$

Then, using (6.8), one can write

$$
{}^{F}\dot{\widehat{p}}_R = B_R\eta, \tag{6.9}
$$

where B_R is a block matrix of the form

$$
B_R = \begin{bmatrix} G \\ -- \\ j \end{bmatrix} \in \Re^{3\times 2},
$$

and the row vector j is given by $j = \left[0 \;\; 1\right] \in \Re^{1\times 2}$.

The path following geometry considered in this paper is illustrated in Fig. 6.1. It is assumed that the path is a smooth planar curve. The coordinate systems Rx_Ry_R and Lx_Ly_L are defined to describe the error kinematics during the path tracking process. The moving reference system Lx_Ly_L is defined such that the x_L-axis is tangent to the path and oriented in the direction of robot motion. The y_R-axis of the robot coordinate system Rx_Ry_R passes through the reference point L associated with the path to follow.

The coordinates and orientation of the frame Lx_Ly_L in the coordinate frame Rx_Ry_R can be expressed in the form

$$
e_{\text{pos}} = T(p_L - p_R), \tag{6.10}
$$

where $e_{\text{pos}} = \begin{bmatrix} x_e & y_e & \psi_e \end{bmatrix}^T \in \Re^3$ is the error posture, x_e is the longitudinal error, y_e is the lateral error, and ψ_e is the orientation error; the posture vector $p_L \in \Re^2 \times S^1$ associated with the reference path is defined as

$$p_L = \begin{bmatrix} x_L & y_L & \psi_L \end{bmatrix}^T, \tag{6.11}$$

where ψ_L is the orientation of the coordinate frame Lx_Ly_L with respect to the fixed frame Fxy, the posture vector p_R is given by (6.8) and the orthogonal matrix $T \in SO(3)$ is given by

$$T = \begin{bmatrix} \cos\psi & \sin\psi & 0 \\ -\sin\psi & \cos\psi & 0 \\ 0 & 0 & 1 \end{bmatrix}.$$

Differentiating (6.10) with respect to time and taking into account the nonholonomic constraints v_{Py}= v_{Ly}=0, (v_{Py} and v_{Ly} are the projections of the velocities of points R and L on the y_R and y_L axes, respectively), and using the fact that $x_e(t) = \dot{x}_e(t) = 0$ after some work, the error kinematics for path following applications is obtained in the form

$$\dot{e} = \varsigma_1(e) + \varsigma_2(e)\omega, \tag{6.12}$$

where $\dot{e} \in \Re^2$ represents the time derivative of $e \in \Re^2$ defined as

$$e = [\, y_e \;\; \psi_e \,]^T, \tag{6.13}$$

$\zeta_1(e)$ and $\zeta_2(e)$ are C^1 vector functions given by

$$\varsigma_1(e) = \begin{bmatrix} v\tan\psi_e & vc_r/\cos\psi_e \end{bmatrix}^T,$$
$$\varsigma_2(e) = \begin{bmatrix} -(y_e\tan\psi_e + {}^P d_x) & -(1 + y_e c_r/\cos\psi_e) \end{bmatrix}^T,$$

v_{Px} is the velocity of mid-point P of the wheel axle, ω is the angular velocity of the robot considered as control variable (input) of the system, and c_r is the curvature of the reference path.

6.2.2 *Robot-Camera Model*

A monocular camera is placed in front of the mobile robot, where the origin of the camera frame $Cx_Cy_Cz_C$ coincides with the center of the coordinate system $Rx_Ry_Rz_R$,

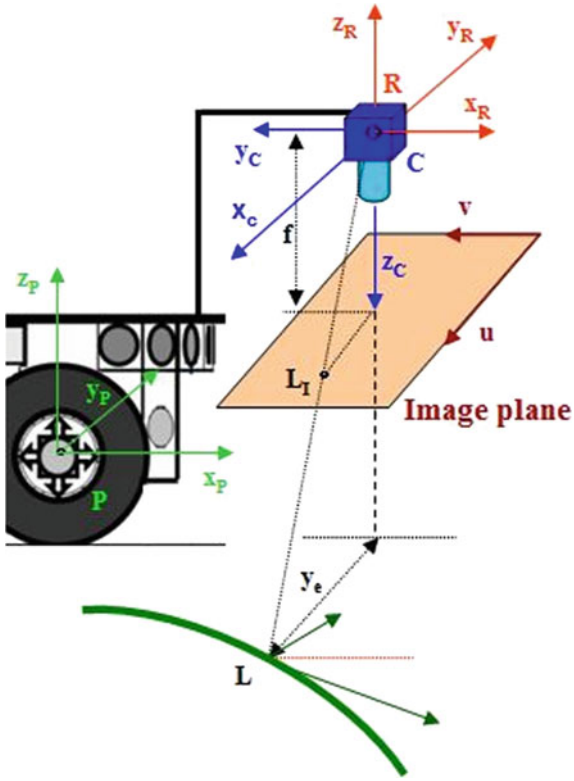

Fig. 6.2 Robot-camera geometry

at distance h from the ground. The optical axis of the camera is perpendicular to the surface of motion, as shown in Fig. 6.2. The focal length of the camera is denoted by f.

The geometric relationships between the onboard camera and a feature point from the reference line are shown in Fig. 6.2. Let us denote the position of a feature point L on the reference line with respect to the camera frame $Cx_Cy_Cz_C$ by ${}^C p_L \in \Re^3$, as follows

$$ {}^C p_L = \begin{bmatrix} {}^C x_L \\ {}^C y_L \\ {}^C z_L \end{bmatrix}. \tag{6.14} $$

The corresponding pixel coordinates ${}^I p_L$ in the pixel coordinate system Iuv fixed to the image plane (Fig. 6.2) are obtained as follows

$$ {}^I p_L = \begin{bmatrix} u_L \\ v_L \\ 1 \end{bmatrix} = \frac{1}{{}^C z_L} T_{\text{int}} {}^C p_L, \tag{6.15} $$

where ${}^{C}z_L = h \in \Re$, $T_{\text{int}} \in \Re^{3\times 3}$ is the intrinsic camera calibration matrix given by

$$T_{\text{int}} = \begin{bmatrix} fs_u & 0 & u_0 \\ 0 & fs_v & v_0 \\ 0 & 0 & 1 \end{bmatrix},$$

(s_u, s_v) are the camera scaling factors and f is the focal length of the camera.

From (6.15), given the pixel coordinates (u_L, v_L), one can determine the coordinates of point L in the camera frame $Cx_Cy_Cz_C$, as follows

$${}^{C}p_L = {}^{C}z_L T_{\text{int}}^{-1}\, {}^{I}p_L.. \tag{6.16}$$

On the other hand, given the coordinates ${}^{C}p_L$ of point L in the camera frame $Cx_Cy_Cz_C$, the coordinates of point L in the robot coordinate frame $Rx_Ry_Rz_R$ are obtained as follows

$${}^{R}p_L = {}^{C}z_L\, {}^{C_1}R_{z_{C1},\pi/2}^{-1} R_{x_C,\pi}^{-1} T_{\text{int}}^{-1}\, {}^{I}p_L, \tag{6.17}$$

where the two consecutive rotation matrices $R_{x_C,\pi} \in SO(3)$ and $R_{z_C,\pi/2} \in SO(3)$ are given by

$$R_{x_C,\pi} = \begin{bmatrix} 1 & 0 & 0 \\ 0 & -1 & 0 \\ 0 & 0 & -1 \end{bmatrix},$$

$$R_{z_C,\pi/2} = \begin{bmatrix} 0 & -1 & 0 \\ 1 & 0 & 0 \\ 0 & 0 & 1 \end{bmatrix}.$$

The lateral error y_e is calculated from the image based on the pixel coordinates in the image plane of the image feature point L_I (Fig. 6.3), corresponding to the feature point L from the reference line on the ground. Knowing the camera intrinsic parameters and the height h of the camera from the ground, the coordinates of a feature point L belonging to the reference line in the robot reference system $Rx_Ry_Rz_R$ can be recovered from its pixel coordinates in the image plane. This error distance is obtained as a difference between the image plane coordinates of the principal point C and the image point L_I, respectively, and is a function of the intrinsic camera parameters and the known distance h from the camera to the ground.

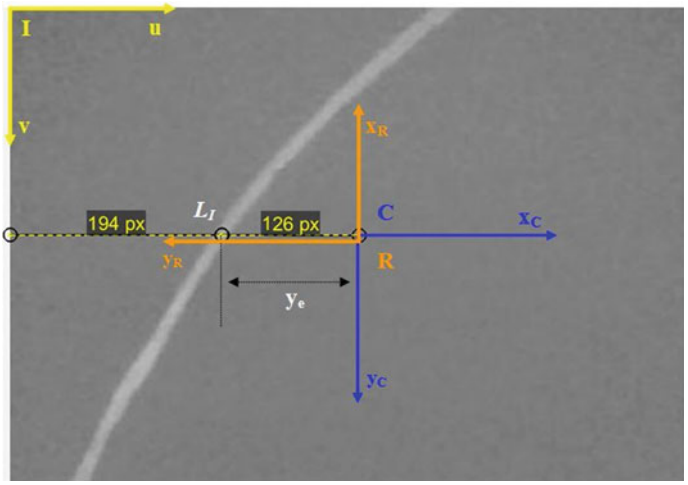

Fig. 6.3 Extraction of a feature point from the line

6.3 Feedback Control Design and Stability Analysis

6.3.1 Circular Line Tracking

Assuming that the reference path is a sequence of circular segments or/and straight lines, and robot velocity v_{Px} is constant and positive (forward robot motion), the path tracking problem consists of finding a feedback control law for the system (6.12) with control input ω, such that the state vector $e = [y_e, \psi_e]^T$ tends to $e_s = [y_{es}, \psi_{es}]^T$ as $t \to \infty$, where y_{es} and ψ_{es} have constant values.

The following feedback control law is proposed

$$\omega = v_{Px} k y_e, \tag{6.18}$$

where k is a positive constant and v_{Px}, (v_{Px}= cte >0), is the robot speed.

Applying (6.18) to (6.12), the resulting nonlinear closed-loop system has the form

$$\dot{e} = v_{Px} \eta_c(e), \tag{6.19}$$

where the vector function η_c given by

$$\eta_c = \begin{bmatrix} -{}^P d_x k y_e (1 - k y_e^2) \tan \psi_e \\ -k y_e + ((1 - k y_e^2)/\cos \psi_e) c_r \end{bmatrix}$$

is continuously differentiable.

The equilibrium point e_s of system (6.19) is at

$$\begin{aligned} e_s &= \begin{bmatrix} y_{es} \\ \psi_{\theta s} \end{bmatrix} \\ &= \begin{bmatrix} \left(-sqrt(1 - {}^P d_x^2 c_r^2) + sqrt(1 - {}^P d_x^2 c_r^2 + 4c_r/k)\right)/2c_r \\ a \sin({}^P d_x c_r) \end{bmatrix}. \end{aligned} \tag{6.20}$$

The stability of the equilibrium point (6.20) for the nonlinear system (6.19) is analyzed by investigating the stability of the linearized system using Lyapunov stability theory [20].

The linearization of the nonlinear system (6.19) at the equilibrium point (6.20) has the form

$$\Delta \dot{e} = v_{Px} M_c \Delta e, \tag{6.21}$$

where the vector $\Delta e \in \Re^2$ is given by

$$\Delta e = \begin{bmatrix} \Delta y_e \\ \Delta \psi_e \end{bmatrix} = \begin{bmatrix} y_e - y_{es} \\ \psi_e - \psi_{es} \end{bmatrix},$$

$M_c \in \Re^{2\times 2}$ is the Jacobian matrix of η_c, (v_{Px}= cte >0) in the form

$$\begin{aligned} M_c &= \left.\frac{\partial \eta_c}{\partial e}\right|_{e=e_s} \\ &= v_{Px} \begin{bmatrix} -k({}^P d_x + y_{es} \tan \psi_{\theta s}) & -k(1 + (c_r y_{es}/\cos \psi_{\theta s})) \\ (1 - k y_{es}^2)/\cos^2 \psi_{\theta s} & \left((1 - k y_{es}^2)/\cos^2 \psi_{\theta s}\right) c_r \end{bmatrix} \\ &= v_{Px} \begin{bmatrix} {}^P d_x m_{21} & m_{12} \\ m_{21} & m_{12} {}^P d_x c_r^2 \end{bmatrix} \end{aligned} \tag{6.22}$$

with

$$\begin{aligned} m_{12} &= (1 - k y_{es}^2)/(1 - {}^P d_x^2 c_r^2) \\ m_{21} &= -k\left[1 + (2 y_{es} c_r)/\text{sqrt}\left(1 - {}^P d_x^2 c_r^2\right)\right] \end{aligned} \tag{6.23}$$

To analyze the stability of linear system (6.21), we test the eigenvalues λ_i, (i =1, 2) of matrix M_c. The characteristic equation of matrix M_c takes the form

$$\begin{aligned} &\lambda^2 - \lambda Tr(M_c) + \det(M_c) \\ &\quad = \lambda^2 - {}^P d_x \left(m_{12} c_r^2 + m_{21}\right)\lambda - m_{12} m_{21}\left(1 - {}^P d_x^2 c_r^2\right). \\ &\quad = 0 \end{aligned} \tag{6.24}$$

In order that the squired Eq. (6.24) does not have any roots with positive real part, it is necessary and sufficient that all its coefficients be of the same sign, which implies that

$$Tr(M_c) < 0 \tag{6.25}$$

and

$$\det(M_c) > 0 \tag{6.26}$$

To be more concrete, consider the case when the curvature of the reference path $c_r = cte > 0$ (analogous results can be obtained when $c_r = cte < 0$), and also the following inequality holds

$$y_{es}c_r + \text{sqrt}\left(1 - {}^{P}d_x^2 c_r^2\right) > 0, \tag{6.27}$$

irrespective of the sign of y_e.

In order to prove that inequality (6.25) holds, the expression for y_{es} from the first equation of (6.20) is substituted into (6.25). Using (6.23), and taking into account that

$$0 < s < 1, \tag{6.28}$$

where

$$s := 1 - {}^{P}d_x^2 c_r^2 > 0, \tag{6.29}$$

after some work, the following inequality is obtained

$$(k/2)\left\{s + \text{sqrt}(s)\text{sqrt}\left[s + \left(4c_r^2/k\right)\right]\right\} > 0, \tag{6.30}$$

which means that the inequality (6.25) holds.

In order to prove that inequality (6.26) holds, using the expression for $\det(M_c)$ from the last coefficient of (6.24), and taking into account that $s > 0$, one has to prove that

$$m_{12}m_{21} < 0. \tag{6.31}$$

Using the first equation from (6.20) for y_{es}, and the expressions for m_{12} and m_{21} given in (6.23), after some work, the following inequality is obtained

$$(1/s)\left[1 + \left(4c_r^2/k\right)\right] - 1 > 0, \tag{6.32}$$

which means that the inequality (6.24) holds.

Based on (6.30) and (6.32), it follows that $Re\lambda_i < 0$, (i =1, 2). Application of the Lyapunov's indirect method [13] indicates that the equilibrium point $[y_{es}, \psi_{es}]^T$ is locally asymptotically stable point for the nonlinear system (6.19).

6.3.2 *Straight-Line Tracking*

In particular, in the case of straight line following (c_r=0 in (6.12)), and applying the feedback control law given by (6.18), the resulting time-invariant closed-loop system (6.19), ($v_{Px} = cte > 0$), has the form

$$\dot{e} = \begin{bmatrix} \dot{y}_e \\ \dot{\psi}_e \end{bmatrix} = v_{Px}\eta_c(e), \tag{6.33}$$

where the vector e is given by (6.13) and the vector function η_c is in the form

$$\eta_C = \begin{bmatrix} -{}^P d_x k y_e (1 - k y_e^2) \tan \psi_e \\ -k y_e \end{bmatrix}.$$

The origin (0, 0) becomes an equilibrium point for the nonlinear system (6.33). After linearizing the system (6.33) around the origin, is obtained

$$\dot{e} = M_s e, \tag{6.34}$$

where the matrix $M_s \in \Re^{2\times 2}$ has the form

$$M_S = \begin{bmatrix} -k\,{}^P d_x v_{Px} & v_{Px} \\ -k v_{Px} & 0 \end{bmatrix}. \tag{6.35}$$

A Lyapunov function for the linear system (6.34) is found by taking a positive definite matrix $Q \in R^{2\times 2}$ of the form (v_{Px}= $cte > 0$)

$$Q = \begin{bmatrix} v_{Px} & 0 \\ 0 & v_{Px} \end{bmatrix} \tag{6.36}$$

and solving for $P \in \Re^{2\times 2}$ the Lyapunov equation

$$P M_s + M_s^T P = -Q. \tag{6.37}$$

The unique solution of the matrix Eq. (6.37) for P is obtained as follows

$$P = \begin{bmatrix} \frac{1+k}{2k\,{}^{P}d_x} & -\frac{1}{2} \\ -\frac{1}{2} & \frac{1}{2k^2\,{}^{P}d_x}\left(1+k+k^2\,{}^{P}d_x\right) \end{bmatrix}. \tag{6.38}$$

The symmetric matrix P is positive definite since its leading principal minors are positive ($k = cte > 0$; ${}^{P}d_x = cte > 0$)

$$\begin{aligned} &\det\left(\frac{1+k}{2k\,{}^{P}d_x}\right) > 0, \\ &\det\begin{bmatrix} \frac{1+k}{2k\,{}^{P}d_x} & -\frac{1}{2} \\ -\frac{1}{2} & \frac{1}{2k^2\,{}^{P}d_x}\left(1+k+k^2\,{}^{P}d_x\right) \end{bmatrix} \\ &= \frac{1+k}{k}\left(\frac{1}{k^2\,{}^{P}d_x^2}+\frac{1}{4k\,{}^{P}d_x^2}+\frac{1}{4}\right)-\frac{1}{4} > 0. \end{aligned} \tag{6.39}$$

Hence, M_c is stability matrix (i.e., $Re\lambda_i < 0$ for the eigenvalues of M_c) for the system (6.34), [20]. Since the robot velocity is assumed to be constant and strictly positive, it follows that using control (6.18) local asymptotic stability of the nonlinear system (6.33) is achieved when the control (6.18) is applied.

6.4 Simulation and Experimental Results

Numerical simulation tests using MATLAB and experiments are carried out in order to validate the proposed path tracking control. The look-ahead distance for the robot reference point R (Fig. 6.1) was chosen to be ${}^{P}d_x = 0.3$ m. The forward robot velocity was chosen to be v_{Px}=0.3 m/s and the controller gain in feedback control given by (6.18) was k_y=10.

For the first simulation, a circular reference path of radius 1 m was assigned. In the first test in circular path following, the initial conditions were chosen to be $e = [\, y_e(0)\ \psi_e(0)\,]^T = [\,-0.3\ -0.3\,]^T$. The path drown by the robot guide point R and evolution in time of the path error coordinates are depicted, respectively, in Fig. 6.4a, b.

For the second simulation test in circular path following, the initial conditions were $e = [\, y_e(0)\ \psi_e(0)\,]^T = [\,0.3\ 0.3\,]^T$. The path drown by the robot guide point R and evolution in time of the path error coordinates is depicted in Fig. 6.4c, d, respectively. As seen from Fig. 6.4b, d, the error coordinates $y_e(t)$ and $\psi_e(t)$ asymptotically tend to the steady-state values given by (6.20), which is in conformity with the stability analysis presented in Sect. 6.3. The steady-state lateral error y_{es} in the both cases is equal to 0.095 m.

For the straight-line path tracking simulation test, the initial conditions were chosen to be $e = [\, y_e(0)\ \psi_e(0)\,]^T = [\,0.25\ 0.1\,]^T$. The path drown by the robot guide point R and evolution in time of the path error coordinates are depicted, respectively, in Fig. 6.5a, b, respectively. The results from the simulation confirmed the analyt-

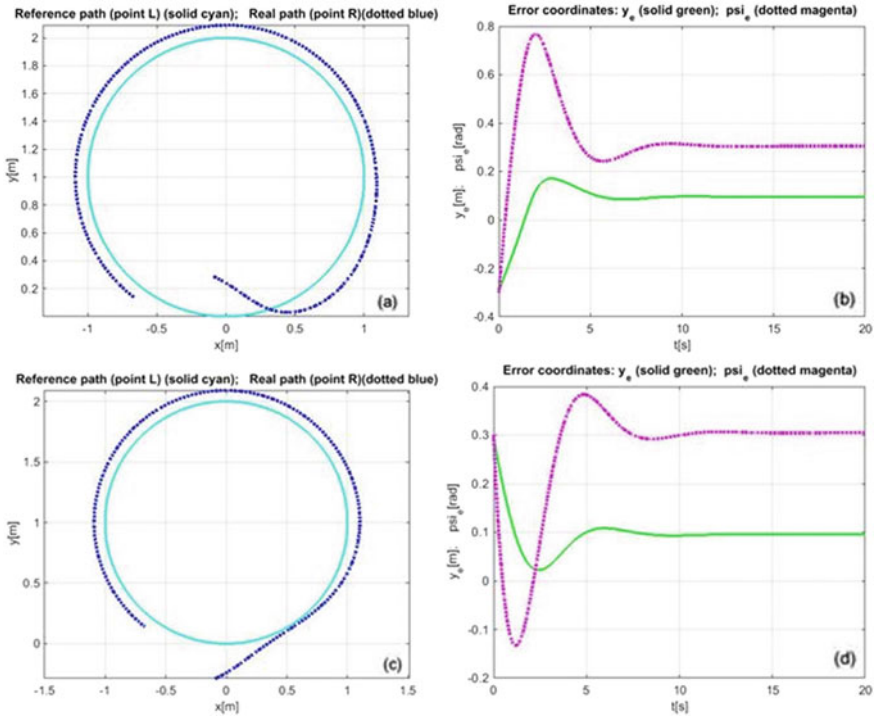

Fig. 6.4 Following a circular path: **a** and **c** planar path drown by the reference point R of the robot (blue dotted line) and reference circular path (cyan solid line); **b** and **d** evolution in time of the error coordinates y_e (green solid line) and ψ_e (magenta dotted line)

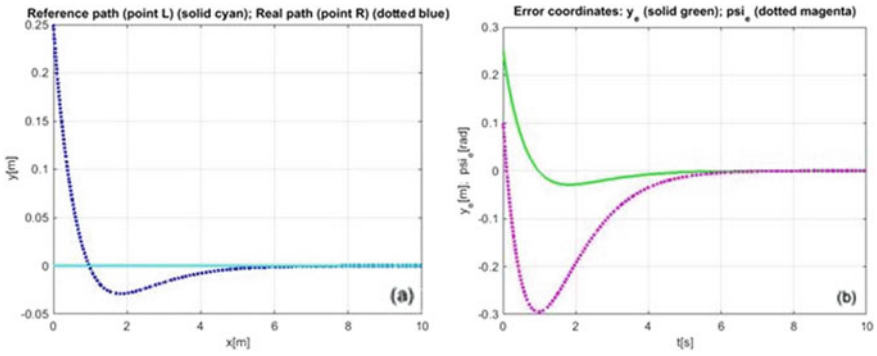

Fig. 6.5 Following a straight-line path: **a** Planar path drown by the reference point R of the robot (blue dotted line) and reference circular path (cyan solid line); **b** Evolution in time of the error coordinates y_e (green solid line) and ψ_e (magenta dotted line)

Fig. 6.6 Experiments in circular line tracking

Fig. 6.7 Experiments in straight-line tracking

ical result obtained in the previous section for straight-line tracking, that the error coordinates y_e and $\psi_e(t)$ asymptotically tend to zero.

Experiments were carried out for tracking a circular and straight-line path using a differential-drive mobile robot Pioneer-3DX equipped with an onboard low cost camera (640 × 480 pixels). For the experiments, the velocity of the robot was set to v_{Px}=0.3 m/s. As seen from Fig. 6.6, the robot was able to follow a circular path with small steady-state lateral error according to (6.20) and without error for straight-line tracking (Fig. 6.7).

6.5 Conclusion

In this paper, a vision-based line following controller for unicycle mobile robots was presented. Using a look-ahead approach, a simple and effective feedback control, which achieves local asymptotic stability of the nonlinear closed-loop system for a circular path with unknown curvature, as well and a straight-line path, was designed and analyzed using Lyapunov stability theory. Simulation and experimental results confirm the validity of the designed vision-based control scheme to perform curved path following in clutter environments with a quite good accuracy.

Acknowledgements This work was supported by the National Science Fund at the Ministry of Education and Science, Republic of Bulgaria, within the project KP-06-H27/16 "Development of Efficient Methods and Algorithms for Tensor-based Processing and Analysis of Multidimensional Images with Application in Interdisciplinary Areas."

References

1. Liaqat, A., Hutabarat, W., Tiwari, D., Tinkler, L.: Autonomous mobile robots in manufacturing: highway code development, simulation, and testing. Int. J. Adv. Manuf. Technol. **104**, 4617–4628 (2019)
2. Sinyukov, D., Padir, T.: Adaptive motion control for a differentially driven semi-autonomous wheelchair platform. In: International Conference on Advanced Robotics, pp. 288–294. IEEE, Istanbul, Turkey (2015)
3. Petrov, P., Nashashibi, F.: Planning and nonlinear adaptive control for an automated overtaking maneuver. In: 14th International IEEE Conference on Intelligent Transportation Systems, pp. 662–667. IEEE, Washington, DC, USA (2011)
4. Palacios, A., Sanchez, A., Bedolla, A., Cordero, J.: The random exploration graph for optimal exploration of unknown environments. Int. J. Adv. Rob. Syst. **14**(1), 1–11 (2017)
5. Rahmat, M., Hudha, K., Idris, A., Amer, N.: Sliding mode control of target tracking system for two degrees of freedom gun turret model. Adv. Military Technol. **11**(1), 13–28 (2016)
6. Calvo, C., Villacorta-Atienza, J., Mironov, V., Gallego, V., Makarov, V.: Waves in isotropic totalistic cellular automata: application to real-time robot navigation. Adv. Complex Syst. **19**(4), 1–18 (2016)
7. Petrov, P., Nashashibi, F.: Saturated feedback control for an automated parallel parking assist system. In: 13th International Conference on Control Automation Robotics and Vision, pp. 577–582. IEEE, Singapore (2014)
8. Ibrahim, F., Abouelsoud, A., Elbab, A., Ogata, T.: Path following algorithm for skid-steering mobile robot based on adaptive discontinuous posture control. Adv. Robot. **33**(9), 439–453 (2019)
9. Emam, M., Fakharian, A.: Solving path following problem for car-like robot in the presence of sliding effect via LMI formulation. J. Comput. Rob. **10**(2), 11–22 (2017)
10. De Luca, A., Oriolo, G., Vendittelli, M.: Control of wheeled mobile robots: an experimental overview. In: Nicosia, S., Siciliano, B., Bicchi, A., Valigi, P. (eds.), LNCIS, vol. 270, pp. 181–226. Springer, Berlin, Heidelberg (2001)
11. Plaskonka, J.: Different kinematic path following controllers for a wheeled mobile robot of (2, 0) type. J. Intell. Rob. Syst. **77**, 481–498 (2015)
12. Petrov, P., Kralov, I.: A look-ahead approach to mobile robot path tracking based on distance-only measurements. AIP Conf. Proc. **2172**, 110005 (2019)
13. Hutchinson, S., Hager, G., Corke, P.: A tutorial on visual servo control. IEEE Trans. Rob. Autom. **12**(6), 651–670 (1996)
14. Cherubini, A., Chaumette, F. Oriolo, G.: A position-based visual servoing scheme for following paths with nonholonomic mobile robots. In: IEEE/RSJ International Conference on Intelligent Robots and Systems, pp. 1648–1654. IEEE, Nice, France (2008)
15. Petrov, P., Georgieva, V.: Vision-based line tracking control for nonholonomic differential-drive mobile robots. In: 9th National Conference with International Participation, ELECTRONICA 2018. IEEE, Sofia, Bulgaria (2018)
16. Kim, S., Oh, S.: Hybrid position and image based visual servoing for mobile robots. J. Intell. Fuzzy Syst. **18**, 73–82 (2007)
17. Corke, P.: Mobile robot navigation as a planar visual servoing problem. In: Jarvis, R., Zelinsky, A. (eds.), Robotics Research, STAR vol. 6, pp. 361–372. Springer, Berlin Heidelberg (2003)
18. Kountchev, R., Mironov, R., Kountcheva, R.: Hierarchical cubical tensor decomposition through low complexity orthogonal transforms. Symmetry **12**(5), 1–17 (2020)
19. Mariottini, G., Oriolo, G., Prattichizzo, D.: Image-based visual servoing for nonholonomic mobile robots using epipolar geometry. IEEE Trans. Rob. **23**(1), 87–100 (2007)
20. Khalil, H.: Nonlinear systems, 3rd edn. Pearson, USA (2002)